frontiers in Materials

ORIGINAL RESEARCH
published: 08 November 2021
doi: 10.3389/fmats.2021.773501

Research on Modeling Crystallographic Texture Evolution of Al Alloy 7075

*Hao Liu, Man Zhao, Yufeng Zhou and Gang Liu**

School of Mechanical and Automotive Engineering, Shanghai University of Engineering Science, Shanghai, China

Crystallographic texture is related to the anisotropy or isotropy of material physical properties, including mechanical performance. The crystallographic effect in micromachining is more significant than that in macro-processing owing to that the depth of the cut and the grain size are in the same order. It is of great significance to model the crystallographic texture evolution induced by mechanical and thermal load during micro-machining to investigate the surface integrity and performance of the finished product. This study performed hot deformation experiments of Al alloy 7075 (AA7075) under various input parameters, including the temperature, temperature rate, stain rate, and strain, which was designed using the Taguchi method. Following that, crystallographic orientation of the samples before and after the deformation was tested using electron back-scattered diffraction (EBSD). Then, the crystallographic texture evolution was modeled with the parameters obtained by fitting a part of the experimental data. The crystallographic texture evolution of AA7075 under different levels of input parameters is studied and analyzed. Finally, the sensitivity of crystallographic orientation evolution to the process parameter is analyzed. The results indicate that these four input parameters have a significant impact on some crystallographic texture of the specimens. The proposed model is instructive in the future investigation of micromachining and microstructure evolution.

Keywords: hot deformation, crystallographic texture, mechanical load, thermal load, EBSD

OPEN ACCESS

Edited by:
Guijian Xiao,
Chongqing University, China

Reviewed by:
Yixuan Feng,
Georgia Institute of Technology, United States
Zishan Ding,
University of Shanghai for Science and Technology, China
Xiang Daohui,
Henan Polytechnic University, China

****Correspondence:***
Gang Liu
liugang@sues.edu.cn

Specialty section:
This article was submitted to Environmental Degradation of Materials, a section of the journal Frontiers in Materials

Received: *10 September 2021*
Accepted: *28 September 2021*
Published: *08 November 2021*

Citation:
Liu H, Zhao M, Zhou Y and Liu G (2021) Research on Modeling Crystallographic Texture Evolution of Al Alloy 7075. Front. Mater. 8:773501. doi: 10.3389/fmats.2021.773501

INTRODUCTION

Aluminum is the most abundant metal material in the Earth's crust. It is easy to process and has high corrosion resistance, electrical conductivity, and thermal conductivity. Alloying aluminum with other elements can obtain better mechanical properties. Alloy aluminum 7075 (AA7075) is used as the main structural material for aviation applications and has been the first choice for the aircraft industry for decades (Yasakau et al., 2014). AA7075, which has high strength-to-density ratio, high ductility, light weight, corrosion resistance, and superior mechanical properties, is widely used in the automotive and aerospace industries (Puchicabrera et al., 2006).

The microstructure of the material includes grain orientation, grain size, dislocation density, and phase transition. During micromachining, the quality of the workpiece will be affected by the microstructure of the workpiece material (Wu et al., 2019). The machining surface quality has an important impact on the performance of the part, and many scholars have done some research around the machining surface quality (Ding et al., 2021). Guo et al. (2021) proposed a new surface roughness prediction system with good prediction performance, which has certain feasibility and

practicality. Li et al. (2021) found that grinding assisted by graphene oxide coolant could improve the surface quality of grinding. The influence mechanism of surface generation and the generation mechanism of residual stress in the grinding process have attracted the attention of many researchers (Li et al., 2019; Ding et al., 2020; Sun et al., 2021; Xiao et al., 2021). For the surface quality requirements of precision machining of complex parts, robotic grinding is also used as a method to control the surface integrity (Lv et al., 2020; Xie et al., 2020; Zhu et al., 2020). The grain orientation is a key parameter in the analysis of the microstructure effect. The study of the evolution of the grain orientation during processing is of great significance for obtaining better machining quality.

The importance of texture in materials science stems from "anisotropy". The properties of single crystals such as mechanical, thermal, magnetic, optical, and chemical can be very different in different crystallographic directions. For example, rotation of the axis of loading can result in a 15% increase in the Young's modulus of commercial pure aluminum from 63 to 72 GPa. Simoneau et al. (2007) through the orthogonal micromachining of normalized AISI 1045 steel and refined AISI 1045 steel found that the small grain size will reduce the maximum plastic strain during chip formation. If the orientation of the grain boundary is not parallel to the shear surface, it can reduce the size of the pits on the processed surface. Cho et al. (2004) studied the effect of initial crystallographic orientation on the microstructure evolution of Ni-30 Fe alloy and found that the development of the deformed microstructure will be affected to a certain extent by the initial grains. Wu et al. (2015) found through copper microcutting experiments that the grain orientation has a great influence on the cutting force and the formation of burrs. The movement direction of the dislocation is obliquely forward of the cutting direction, which is beneficial to reduce the cutting force and the formation of burrs. Lin and Shiu (2016) used molecular dynamics methods to study the nanogrooving of single-crystal copper, and the results showed that the grain orientation has a significant effect on the cutting force and groove morphology. As a typical micro-part processing technology, microgrinding will be significantly influenced by the microstructure effect of the workpiece material. Min et al. (2006) used the tool at different angles relative to the workpiece direction to micro grind face centered cubic (FCC) single crystal materials and found that due to different crystal grain orientations, the activated slip system is different, which will have a significant effect on the surface and edges. Zhao et al. (2021) found that the grain orientation has a significant effect on the residual stress of microgrinding. Aicheler (2010) found that [111] surface grains produced much greater damage and roughness than the oriented surface grains in [100] through surface thermal fatigue experiments of polycrystalline copper. This is because the grains of the two orientations of <111> and <100> had different evolution during the thermal fatigue test of polycrystalline copper, and the surface with a grain orientation of <111> was severely deformed, while the surface with a grain orientation of <100> remained almost unchanged (Aicheler et al., 2011).

The texture evolution of aluminum alloys is mainly caused by the rotation of the operating slip system towards the direction of the applied external force. Also, twinning is considered to contribute to the texture evolution of AA7075 (Tabei 2015). Zhang and Li (2008) studied the grain orientation evolution of extruded magnesium alloy AZ31B sheets under uniaxial stretching at room temperature and found that the twin behavior is also different due to different initial orientations of the grains. Fang et al. (2011) carried out tensile tests on high manganese TWIP steel at different temperatures and found that temperature has a certain effect on the grain orientation evolution and twinning. Chen et al. (2018) studied the effect of strain rate and temperature caused by friction during high-speed sliding on the evolution of copper microstructure, and the results showed that the deformation is dominated by dislocation movement and twinning at lower or higher strain rates. Peng et al. (2018) conducted a uniaxial tensile test on a pure copper sample. In the experiment, with the increase of strain, the crystal grains with orientation <110> gradually rotated to the <111> orientation, and finally found that there were three main grain orientations. The ratio of <111> oriented grains increased significantly, the ratio of <110> oriented grains decreased significantly, and the ratio of <100> oriented grains hardly changed. Sun et al. (2019) studied the Cu-Sn low-temperature TLP-bonding solder joints and observed the grain orientation of the samples at 235, 250, and 265°C reflow and found that Cu_6Zn_5 and Cu_3Zn grains showed the preferential orientations of [001] and [100]. Parajuli et al. (2018) found that after annealing the gold film along the <111> direction, the grain orientation changed significantly. The proportion of <111> oriented grains increased from 50 to 70% because <111> is the preferred orientation of the gold film under certain conditions.

Zhang et al. (2018) conducted stress fracture experiments on Waspaloy alloy and found that the grain orientation evolution behavior is related to the initial grain size of the sample. Zhang et al. (2021) conducted cold rolling experiments on ultra-thin grain-oriented silicon steel and found that changing the shear distribution during the rolling process would change the evolution of grain orientation. Wang et al. (2021) combined the VPSC model and the finite element cutting simulation model to study the texture changes during Ti-6Al-4V processing and found that the slip system plays an important role in the formation of shear texture. Gong et al. (2017) studied the effect of microgrinding parameters on the ground surface and microstructure through a nickel-based single-crystal superalloy microgrinding experiment. Riyad et al. (2021) established a simulation framework based on multilevel crystal plasticity to study the texture evolution of Ti-6Al-4V in tension and compression. Tang et al. (2019) considered thermo-mechanical effects and established a viscoplastic self-consistent model based on dislocation density and introduced it into the hot extrusion process of magnesium alloy bars to analyze the changes in the microstructure. Roatta et al. (2021) used a polycrystalline plastic viscoplastic self-consistent (VPSC) model based on an affine linearization procedure to analyze the crystallographic texture evolution of Zn–Cu–Ti alloy sheets under simple shear and uniaxial tension.

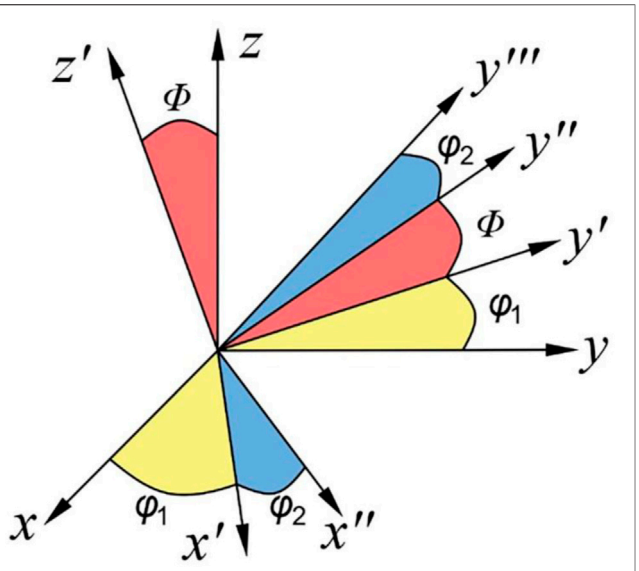

FIGURE 1 | Schematic illustration of Euler angles defined by Bunge's notation.

Researchers concur that crystallographic texture evolutions are important microstructural evolutions occurring in the processing of materials. The above literature mentioned several experimental observations of the abovementioned phenomena. To the best of my belief, the predictive model of crystallographic texture evolution is not presented, which takes the effect of strain rate, strain, temperature, and temperature rate induced by the thermal-mechanical load in machining of different types of metals and alloys. This work focused on analytically modeling the crystallographic texture evolution in microgrinding of AA7075 and developed an empirical model considering the effect of the strain rate, strain, temperature, and temperature rate with the parameters obtained by fitting the experimental data.

CRYSTALLOGRAPHIC TEXTURE EVOLUTION MODELING

Representation of Crystallographic Texture

AA7075 is a FCC metal, and there is no phase transformation in the microgrinding process. The texture research of materials is mainly focused on microtexture analysis. Electron backscatter diffraction (EBSD) is the main tool for microtexture analysis.

Euler angles are about Cartesian axes of the rotation required, and it can be obtained in the desired direction from a reference direction. The work follows Bunge's notation; the Euler angles are represented by φ_1, Φ, and φ_2. The definition of Bunge's notation is shown in **Figure 1**. In order to get to the desired orientation, φ_1 is rotated around the z axis. Φ is rotated around the x axis that has already been rotated, as shown by x' in **Figure 1**. φ_2 is the rotation about the z' axis (the z axis after the first two rotations).

Each crystallite's orientation coordinates are called the "crystal" frame. In Bunge's notation of Euler angles, the range of φ_1 and φ_2 is [0, 2π] while the range of Φ is [0, π].

Modeling of Crystallographic Texture Evolution

Experimental results show that twinning is mostly suppressed in FCC metals such as aluminum, and the major mechanism of inelastic deformation is slip (Barlat et al., 1997). The reason for the change of the crystallographic orientation in slip deformation is explained by Schmid's law (Schmid and Boas 1950). From the perspective of thermodynamics, the direction of the normal slip plane (n) of the crystal should be consistent with the direction of the externally applied load(s). The activation of any slip system requires that the shear stress acting on the slip system to reach a critical value, the so-called "critical resolved shear stress" or τ_{CRSS}. Eshelby proposed the strain and rotation fields in the ellipsoidal grain (Eshelby 1957). Therefore, the rotation of each grain can be determined. Following that, "self-consistent" approaches were introduced to solve the crystal plasticity problem (Hutchinson 1970). The spin (rotation rate) $\mathbf{\Omega}_{ij}^{c}$ of the crystal explains that the crystallographic texture evolution can be found using the following formula:

$$\Omega_{ij}^{c} - \bar{\Omega}_{ij} = \prod : S^{-1} : \left(\dot{\varepsilon}_{ij}^{c} - \bar{\dot{\varepsilon}}_{ij}\right), \tag{1}$$

where S is the fourth-order Eshelby tensor that is only a function of the shape of the ellipsoid particle, and $\prod$ is the skew-symmetric fourth-order Eshelby tensor (Eshelby 1957). $\dot{\varepsilon}_{ij}^{c}$ is the strain rate in the crystal; the overline denotes the value of the medium. The self-consistent approach leads to the following (Molinari et al., 1987):

$$\dot{\varepsilon}_{ij}^{c} - \bar{\dot{\varepsilon}}_{ij} = \bar{M}^{c} : (\sigma^{c} - \bar{\sigma}), \tag{2}$$

where $\bar{M}^{c}$ is the secant modulus associated with the rate.

Feng et al. (2018) used the modified Johnson–Cook flow stress law to calculate the cutting and plowing forces considering the grain size and proposed an analytical model for predicting the milling temperature of Inconel 718 considering the effect of dynamic recrystallization. In this study, we consider only the effect of grain orientation. In this process, the hardening behavior of the material is taken into account and is used to update τ_{CRSS}. The Johnson–Cook model can be used to obtain the constitutive behavior of AA7075 at each temperature.

$$\sigma = (A + B\varepsilon^{n})\left(1 + C\ln\frac{\dot{\varepsilon}}{\dot{\varepsilon}_0}\right)\left(1 - \left(\frac{T_0 - T_w}{T_m - T_w}\right)^{m}\right), \tag{3}$$

where A, B, C, m, n, and $\dot{\varepsilon_0}$ are material constants, ε is the plastic strain, $\dot{\varepsilon}$ is the plastic strain rate, T_0 is the workpiece temperature, T_w is the ambient temperature, and T_m is the material melting

TABLE 1 | Johnson–Cook model parameters for Al Alloy 7075.

A (MPa)	*B* (MPa)	*C*	*m*	*n*	T_m(°C)	$\dot{\varepsilon}_0$ (s^{-1})
520	477	0.001	1	0.52	619.85	5×10^{-4}

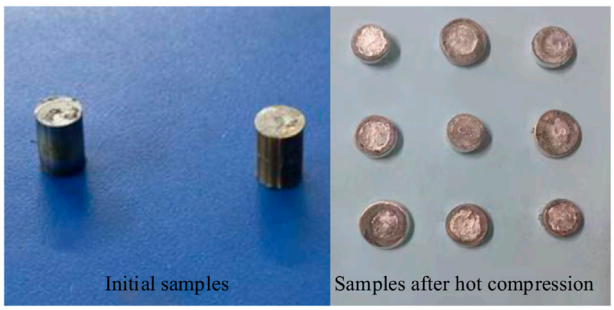

FIGURE 2 | Samples before and after the hot compression test.

temperature. The values of Johnson–Cook model parameters are from Flores-Johnson et al. (2014) in **Table1**.

From the theoretical analysis, it is captured that crystallographic texture evolution is related to the strain rate, strain, temperature, and temperature rate. Therefore, the empirical model can be expressed as follows:

$$\Omega_{ij}^{C} = f\left(T, \dot{T}, \dot{\varepsilon}, \varepsilon\right). \tag{4}$$

For polycrystalline material, crystallographic texture is represented by COs and the corresponding orientation distribution functions (ODFs). Crystallographic texture evolution can be represented by the ODF variation of main COs, as follows:

$$f_{(\varphi_1, \varnothing, \varphi_2)} = a_{k1} T^{a_{k2}} \dot{T}^{a_{k3}} \dot{\varepsilon}^{a_{k4}} \varepsilon^{a_{k5}}, \tag{5}$$

where a_{ij} is the constant and exponents.

To convert the nonlinear model to a linear model, logarithmic transformation is used.

$$\ln f_{(\varphi_1, \varnothing, \varphi_2)} = \ln a_{k1} + a_{k2} \ln T + a_{k3} \ln \dot{T} + a_{k4} \ln \dot{\varepsilon} + a_{k5} \ln \varepsilon . \tag{6}$$

For model simplification, Eq. (6) can be given as follows:

$$y = \beta_0 + \beta_1 A + \beta_2 B + \beta_3 C + \beta_4 D + \delta, \tag{7}$$

where y is logarithmic transformations of the measured surface roughness, and A, B, C, and D are temperature, temperature rate, strain rate, and strain on a logarithmic scale, respectively; β_0, β_1, β_2, β_3, etc., are coefficients to be estimated by the least squares method, and δ is the randomly distributed error terms.

EXPERIMENTS METHOD

Hot Compression Test

In the research process, AA7075 is used as the experimental material. The dimension of samples is a diameter of 8 mm and the height of 12 mm as shown in **Figure 2**.

In order to simulate the microgrinding process and study the flow behavior and crystallographic texture evolution of AA7075, the isothermal compression test was carried out on the G1eeble-3800 thermo-mechanical simulator as shown in **Figure 3**, and each parameter was set to 3 levels, respectively; the temperature was 350, 400, and 450°C, and the temperature rate was 1, 10, and 100°C/s; the strain rate was 0.01, 0.1, and 1 s-1, and the strain was 0.5, 0.6, and 0.7. The hot compression tests were designed according to the Taguchi method, as shown in **Table 2**.

The G1eeble-3800 thermo-mechanical simulator is composed of a computer control system, mechanical control system, and thermal control system, which can simulate various thermal-mechanical processes, such as thermal tension, thermal compression, and plane deformation. For the hot compression test, each sample was heated to the target temperature according to the respective set temperature rate in **Table 1** and then held for 2 min, after which the specimens were compressed according to the respective corresponding strain rate and strain.

The details of the hot compression process are shown in **Figure 4**.

Microstructure Observation

To study the microstructure evolution during hot compression, the microstructure of the samples before and after the test was observed by EBSD. The surface of the compressed sample was polished before the EBSD examination. EBSD data were taken from the center of the polished surface. The samples were polished and tested as depicted in **Figure 5**.

RESULTS AND DISCUSSION

EBSD Measurement Result

Inverse pole diagrams (IPFs) of nine samples were obtained from EBSD, as shown in **Figure 6**, which can be used as a qualitative description of microtexture.

The COs and the corresponding distributions of the nine samples were analyzed by TSL OIM Data Collection 5 software and depicted by the OIM micrographs, as shown in **Figure 7**.

The ODF is a preferred orientation representation of the three-dimensional spatial distribution of a crystal and represents the

FIGURE 3 | G1eeble-3800 compression test setup.

TABLE 2 | Parameter details in the hot compression test.

NO. \ Factors	Temperature rate (°C/s)	Temperature (°C)	Strain rate (s^{-1})	Deformation (um)
1	1	350	0.01	50
2	1	400	0.1	60
3	1	450	1	70
4	10	350	0.1	70
5	10	400	1	50
6	10	450	0.01	60
7	100	350	1	60
8	100	400	0.01	70
9	100	450	0.1	50

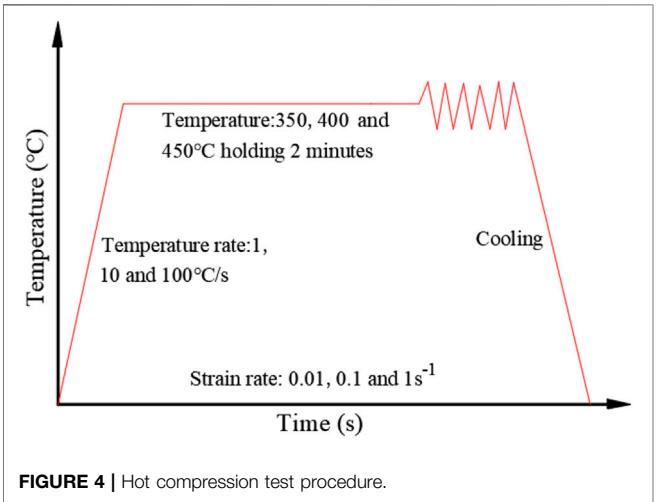

FIGURE 4 | Hot compression test procedure.

odds of a particular crystal orientation defined by the Euler angles. The COs and the corresponding ODFs of the nine samples were obtained by EBSD tests. The top 11 ODFs and COs are listed in **Table 3**.

For comparing the variance of microtexture intuitively, the ODFs of nine specimens are described in **Figure 8**.

Form **Figure 8**, it is found that the ODFs of specimens are completely different, which indicates that crystallographic texture evolution is conspicuous.

The Linear Regression Analysis

In the research process, the crystallographic texture evolution is represented by the main COs evolution of specimens. To determine the main COs, the calculated method was developed. In the method, the ODF variation of each CO is obtained by calculating the difference value between the specimens before and after hot deformation. Then, the sum for ODF variation of each CO was calculated, and the top three variations represent COs evolution. The ODF variation of each specimen is listed in **Table 4**.

It is found that the top three COs are (270.0, 35.3, and 45.0), (35.3, 90.0, and 45.0), and (270.0, 25.2, and 45.0). To connect the crystallographic texture evolution to the process parameters of hot deformation intuitively, the process parameters and ODF variation of the top three COs are listed in **Table 5**.

The coefficients of the three CO evolutions are determined by fitting predictions with 9 groups of experimental data, with the R-squares of 0.8460, 0.9575, and 0.7064, respectively.

$$f_{(270.0,\ 35.3,45.0)} = -4.1189T^{0.0536}\dot{T}^{0.9495}\dot{\varepsilon}^{0.0202}\varepsilon^{0.6141},$$
$$f_{(35.3,90,45.0)} = -10.0246T^{0.1197}\dot{T}^{2.4915}\dot{\varepsilon}^{0.0619}\varepsilon^{1.6069},$$
$$f_{(270.0,25.2,45.0)} = 25.9283T^{-0.0372}\dot{T}^{-7.1702}\dot{\varepsilon}^{0.2640}\varepsilon^{-4.7421}.$$

Sensitive Analysis

The sensitivity analysis of crystallographic orientation evolution to the parameters of the hot deformation process was carried out to investigate the significance of input parameters. Four input

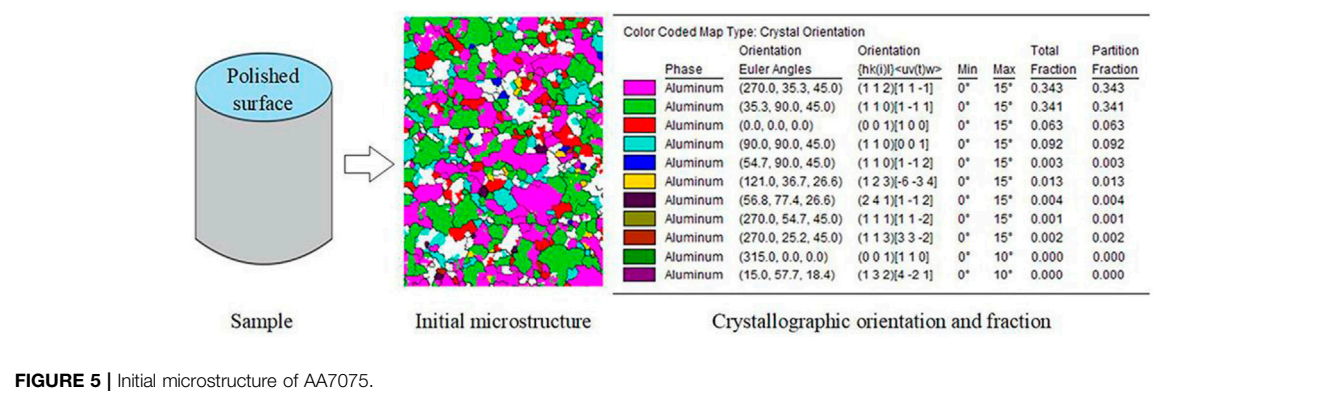

FIGURE 5 | Initial microstructure of AA7075.

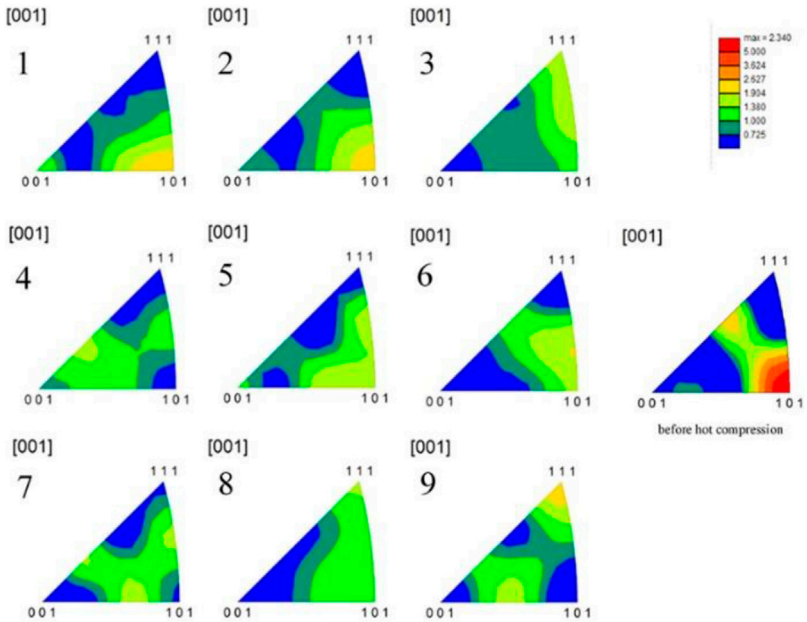

FIGURE 6 | Inverse pole figures of AA7075.

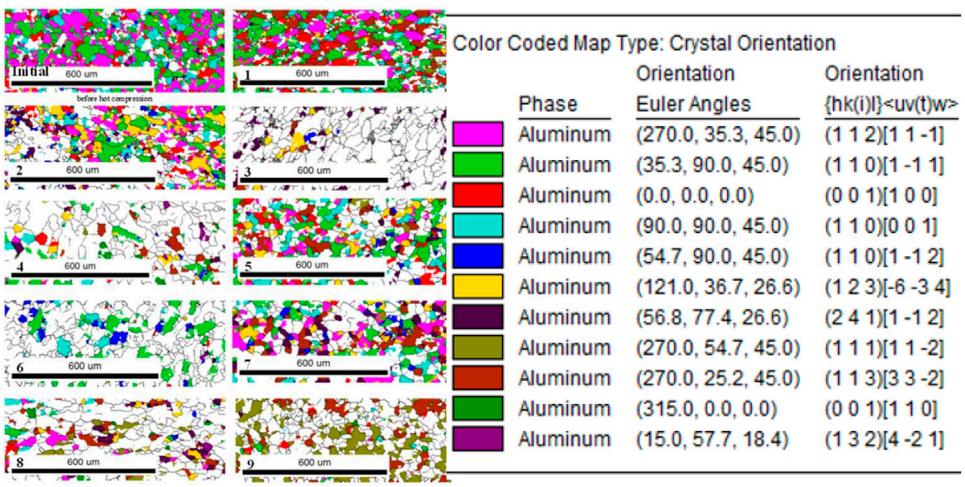

FIGURE 7 | The COs and the corresponding distributions.

parameters were selected for sensitivity analysis, including temperature, temperature rate, strain rate, and strain. The influence of each main input on the three crystallographic orientations (270.0, 35.3, 45.0), (35.3, 90.0, 45.0), and (270.0, 25.2, 45.0) was shown in **Figure 9**.

The results show that the process parameters have a greater impact on the crystallographic orientation evolution within the scope of the experimental exploration. The three crystallographic orientations (270.0, 35.3, 45.0), (35.3, 90.0, 45.0), and (270.0, 25.2, 45.0) have negative correlation with temperature, temperature rate, and strain. The grain orientations of (270.0, 35.3, 45.0) and (35.3, 90.0, 45.0) also show negative correlation with the strain rate, while grain orientations of (270.0, 25.2, and 45.0) are positively correlated with the strain rate. Therefore, to obtain the two crystallographic orientations (270.0, 35.3, 45.0) and (35.3, 90.0, 45.0), lower temperature, temperature rate, strain rate, and the strain are required. To obtain crystallographic orientation of (270.0, 25.2, 45.0), low temperature, small temperature rate, small strain, and large strain rate are required. At the same time, it can be seen that the effect of temperature on the evolution of grain orientation is almost linear, and as the strain rate increases, the rate of grain orientation evolution slows down.

TABLE 3 | The COs and the corresponding ODFs of specimens.

Bunge Euler angles $(\varphi_1, \varnothing, \varphi_2)$	**ODF**									
Specimen	Initial	NO.1	NO.2	NO.3	NO.4	NO.5	NO.6	NO.7	NO.8	NO.9
(270.0, 35.3, 45.0)	0.343	0.144	0.109	0.000	0.014	0.047	0.000	0.047	0.010	0.003
(35.3, 90.0, 45.0)	0.341	0.262	0.171	0.002	0.078	0.123	0.053	0.110	0.022	0.018
(0.0, 0.0, 0.0)	0.063	0.069	0.062	0.002	0.018	0.047	0.008	0.025	0.001	0.021
(90.0, 90.0, 45.0)	0.092	0.078	0.059	0.002	0.015	0.065	0.010	0.031	0.038	0.021
(54.7, 90.0, 45.0)	0.003	0.004	0.025	0.008	0.006	0.028	0.014	0.016	0.045	0.001
(121.0, 36.7, 26.6)	0.013	0.031	0.127	0.019	0.032	0.085	0.002	0.041	0.020	0.004
(56.8, 77.4, 26.6)	0.004	0.007	0.028	0.044	0.008	0.051	0.006	0.059	0.048	0.015
(270.0, 54.7, 45.0)	0.001	0.025	0.012	0.001	0.008	0.036	0.014	0.074	0.022	0.173
(270.0, 25.2, 45.0)	0.002	0.154	0.054	0.020	0.070	0.082	0.000	0.083	0.012	0.107
(315.0, 0.0, 0.0)	0.000	0.000	0.000	0.002	0.003	0.000	0.000	0.000	0.006	0.001
(15.0, 57.7, 18.4)	0.000	0.001	0.002	0.014	0.003	0.002	0.001	0.001	0.054	0.000

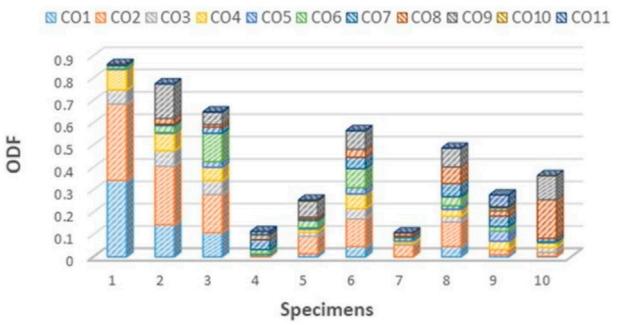

FIGURE 8 | The ODF of specimens after hot deformation.

CONCLUSION

This article mainly studies the crystallographic orientation evolution of Al alloy 7075 under mechanical and thermal loads. The Taguchi method was used to conduct hot compression tests on Al alloy 7075 samples at different temperatures, temperature rates, strains, and strain rates, and the COs and the corresponding ODFs are measured by the EBSD tests. The crystallographic texture evolution was modeled using the parameters obtained by the fitting part of the experimental data. The model linked the crystallographic texture evolution with the hot deformation process parameters to study the crystallographic texture evolution of Al Alloy 7075 under force-thermal loading. The following conclusions are drawn from this study:

1) The surface of Al Alloy 7075 sample had different crystallographic texture evolutions under the hot compression test with four different levels of parameter combination.
2) For the top three crystallographic orientations of the ODF variation, with the increase of temperature, temperature rate, strain rate, and strain, the grain orientations of (270.0, 35.3, 45.0) and (35.3, 90.0, 45.0) decrease, and oriented grains of (270.0, 25.2, 45.0) decrease with the increase of temperature, temperature rate, and strain, but there is a positive correlation with the strain rate.
3) The effect of temperature on the evolution of grain orientation is almost linear, and as the strain rate increases, the rate of grain orientation evolution slows down.
4) The thermo-mechanical load in micromachining is closely related to the process parameters. This study will be instructive for the crystallographic texture evolution in micromachining. This paper focuses on crystallographic orientation evolution under the thermo-mechanical load, and it is important to examine the

TABLE 4 | The ODF variation of each specimen.

Bunge Euler angles $(\varphi_1, \varnothing, \varphi_2)$	**ODF variation**									
Specimen	NO.1	NO.2	NO.3	NO.4	NO.5	NO.6	NO.7	NO.8	NO.9	Sum
(270.0, 35.3, 45.0)	0.199	0.234	0.343	0.329	0.296	0.343	0.296	0.333	0.34	2.713
(35.3, 90.0, 45.0)	0.079	0.17	0.339	0.263	0.218	0.288	0.231	0.319	0.323	2.23
(0.0, 0.0, 0.0)	0.006	0.001	0.061	0.045	0.016	0.055	0.038	0.062	0.042	0.326
(90.0, 90.0, 45.0)	0.014	0.033	0.09	0.077	0.027	0.082	0.061	0.054	0.071	0.509
(54.7, 90.0, 45.0)	0.001	0.022	0.005	0.003	0.025	0.011	0.013	0.042	0.002	0.124
(121.0, 36.7, 26.6)	0.018	0.114	0.006	0.019	0.072	0.011	0.028	0.007	0.009	0.284
(56.8, 77.4, 26.6)	0.003	0.024	0.04	0.004	0.047	0.002	0.055	0.044	0.011	0.23
(270.0, 54.7, 45.0)	0.024	0.011	0	0.007	0.035	0.013	0.073	0.021	0.172	0.356
(270.0, 25.2, 45.0)	0.152	0.052	0.018	0.068	0.08	0.002	0.081	0.01	0.105	0.568
(315.0, 0.0, 0.0)	0	0	0.002	0.003	0	0	0	0.006	0.001	0.012
(15.0, 57.7, 18.4)	0.001	0.002	0.014	0.003	0.002	0.001	0.001	0.054	0	0.078

TABLE 5 | The process parameters and ODF variation of the top three COs.

Factors / NO.	Temperature rate (°C/s)	Temperature (°C)	Strain rate (s^{-1})	Deformation (μm)	Bunge Euler angles (φ_1, $\varnothing$, φ_2)		
					(270.0, 35.3, 45.0)	(35.3, 90.0, 45.0)	(270.0, 25.2, 45.0)
1	1	350	0.01	50	0.199	0.079	0.152
2	1	400	0.1	60	0.234	0.17	0.052
3	1	450	1	70	0.343	0.339	0.018
4	10	350	0.1	70	0.329	0.263	0.068
5	10	400	1	50	0.296	0.218	0.08
6	10	450	0.01	60	0.343	0.288	0.002
7	100	350	1	60	0.296	0.231	0.081
8	100	400	0.01	70	0.333	0.319	0.01
9	100	450	0.1	50	0.34	0.323	0.105

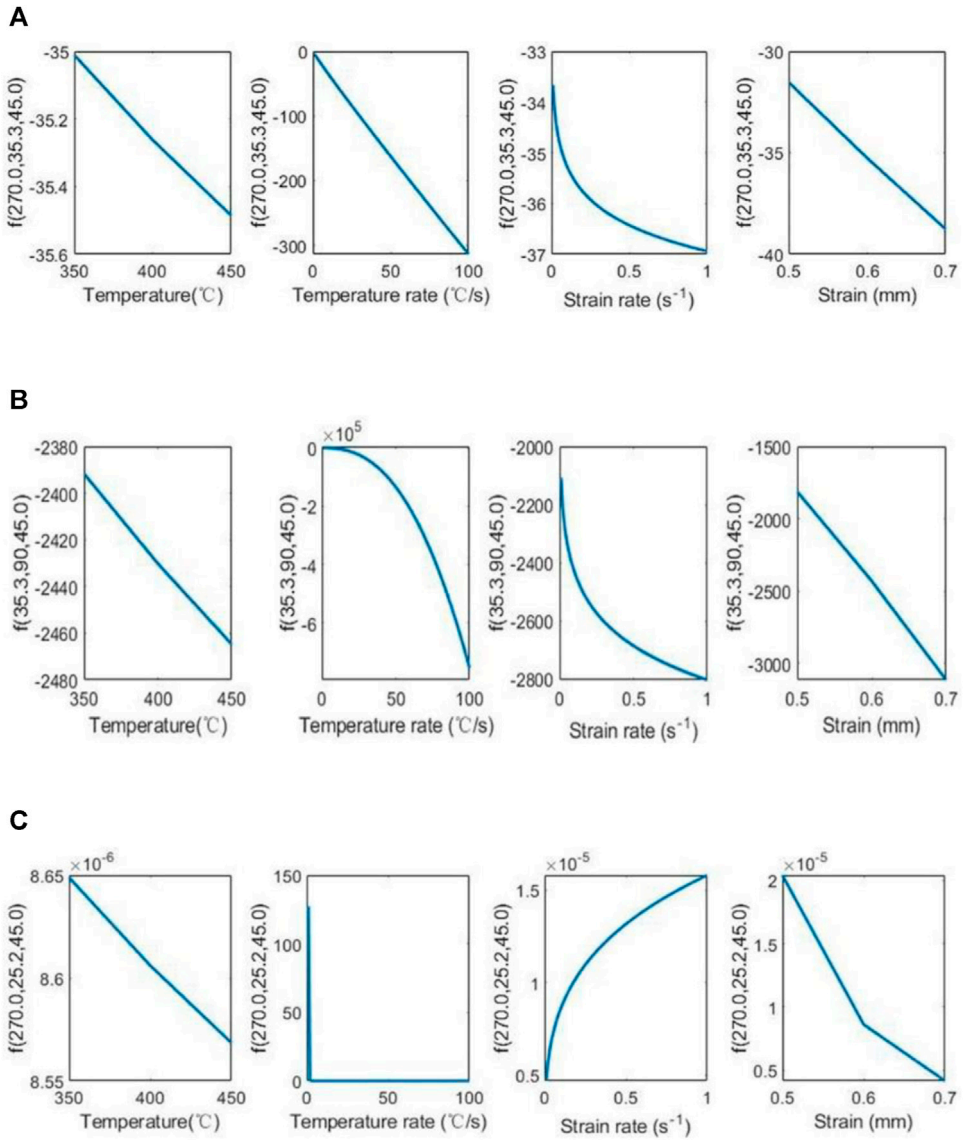

FIGURE 9 | Sensitivity analysis of the main effects on **(A)** (270.0, 35.3, 45.0), **(B)** (35.3, 90.0, 45.0), and **(C)** (270.0, 25.2, 45.0) orientations.

evolution of other material microstructures evolution such as grain size and recrystallization in future studies.

DATA AVAILABILITY STATEMENT

The raw data supporting the conclusion of this article will be made available by the authors, without undue reservation.

AUTHOR CONTRIBUTIONS

MZ, HL, and YZ contributed to conception and design of the study. MZ and HL participated in the experimental data acquisition and data analysis. HL wrote the first draft of the manuscript. MZ, GL, and YZ wrote sections of the manuscript. All authors contributed to manuscript revision, read, and approved the submitted version.

FUNDING

This work was supported by the Shanghai Pujiang Program (20PJ1404700) and the Young Scientific Research Team Cultivation Program of SUES (QNTD202112).

REFERENCES

Aicheler, M. (2010). Influence of Grain Orientation on Evolution of Surface Features in Fatigued Polycrystalline Copper: A Comparison of thermal and Uniaxial Mechanical Fatigue Results, *J. Phys. Conf. Ser.* 240, 012051. doi:10.1088/1742-6596/240/1/012051

Aicheler, M., Sgobba, S., Arnau-Izquierdo, G., Taborelli, M., Calatroni, S., Neupert, H., et al. (2011). Evolution of Surface Topography in Dependence on the Grain Orientation during Surface thermal Fatigue of Polycrystalline Copper. *Int. J. Fatigue* 33 (3), 396–402. doi:10.1016/j.ijfatigue.2010.09.015

Barlat, F., Becker, R. C., Hayashida, Y., Maeda, Y., Yanagawa, M., Chung, K., et al. (1997). Yielding Description for Solution Strengthened Aluminum Alloys. *Int. J. Plasticity* 13 (4), 385–401. doi:10.1016/S0749-6419(97)80005-8

Chen, X., Schneider, R., Gumbsch, P., and Greiner, C. (2018). Microstructure Evolution and Deformation Mechanisms during High Rate and Cryogenic Sliding of Copper. *Acta Materialia* 161, 138–149. doi:10.1016/j.actamat.2018.09.016

Cho, J.-Y., Inoue, T., Yin, F., and Nagai, K. (2004). Effect of Initial Grain Orientation on Evolution of Deformed Microstructure in Hot Compressed Ni-30Fe Alloy. *Mater. Trans.* 45 (10), 2960–2965. doi:10.2320/matertrans.45.2960

Ding, Z., Sun, G., Guo, M., Jiang, X., Li, B., and Liang, S. Y. (2020). Effect of Phase Transition on Micro-grinding-induced Residual Stress. *J. Mater. Process. Tech.* 281, 116647. doi:10.1016/j.jmatprotec.2020.116647

Ding, Z., Sun, J., Guo, W., Jiang, X., and Wu C, L. S. Y. (2021). Thermal Analysis of 3J33 Grinding under Minimum Quantity Lubrication Condition. *Int. J. Precision Eng. Manufacturing-Green Tech.* doi:10.1007/s40684-021-00391-y

Eshelby, J. D. (1957). The Determination of the Elastic Field of an Ellipsoidal Inclusion, and Related Problems. *Proc. R. Soc. Lond.* 241 (1226), 376–396. doi:10.1098/rspa.1957.0133

Fang, X.-H., Yang, P., Lu, F.-Y., and Meng, L. (2011). Dependence of Deformation Twinning on Grain Orientation and Texture Evolution of High Manganese TWIP Steels at Different Deformation Temperatures. *J. Iron Steel Res. Int.* 18 (11), 46–52. doi:10.1016/s1006-706x(11)60116-7

Feng, Y., Pan, Z., and Liang, S. Y. (2018). Temperature Prediction in Inconel 718 Milling with Microstructure Evolution. *Int. J. Adv. Manuf Technol.* 95 (9-12), 4607–4621. doi:10.1007/s00170-018-1581-1

Flores-Johnson, E. A., Shen, L., Guiamatsia, I., and Nguyen, G. D. (2014). Numerical Investigation of the Impact Behaviour of Bioinspired Nacre-like Aluminium Composite Plates. *Composites Sci. Tech.* 96, 13–22. doi:10.1016/j.compscitech.2014.03.001

Gong, Y., Zhou, Y., Wen, X., Cheng, J., Sun, Y., and Ma, L. (2017). Experimental Study on Micro-grinding Force and Subsurface Microstructure of Nickel-Based Single crystal Superalloy in Micro Grinding. *J. Mech. Sci. Technol.* 31 (7), 3397–3410. doi:10.1007/s12206-017-0629-8

Guo, W., Wu, C., Ding, Z., and Zhou, Q. (2021). Prediction of Surface Roughness Based on a Hybrid Feature Selection Method and Long Short-Term Memory Network in Grinding. *Int. J. Adv. Manuf Technol.* 112 (9-10), 2853–2871. doi:10.1007/s00170-020-06523-z

Hutchinson, J. W. (1970). Elastic-plastic Behaviour of Polycrystalline Metals and Composites. *Proc. R. Soc. Lond.* 319 (1537), 247–272. doi:10.1098/rspa.1970.0177

Li, C., Li, X., Huang, S., Li, L., and Zhang, F. (2021). Ultra-precision Grinding of Gd3Ga5O12 Crystals with Graphene Oxide Coolant: Material Deformation Mechanism and Performance Evaluation. *J. Manufacturing Process.* 61, 417–427. doi:10.1016/j.jmapro.2020.11.037

Li, C., Li, X., Wu, Y., Zhang, F., and Huang, H. (2019). Deformation Mechanism and Force Modelling of the Grinding of YAG Single Crystals. *Int. J. Machine Tools Manufacture* 143, 23–37. doi:10.1016/j.ijmachtools.2019.05.003

Lin, Y. C., and Shiu, Y. C. (2016). Effect of Crystallographic Orientation on Single crystal Copper Nanogrooving Behaviors by MD Method. *Int. J. Adv. Manuf Technol.* 89 (9-12), 3207–3215. doi:10.1007/s00170-016-9282-0

Lv, Y., Peng, Z., Qu, C., and Zhu, D. (2020). An Adaptive Trajectory Planning Algorithm for Robotic belt Grinding of Blade Leading and Trailing Edges Based on Material Removal Profile Model. *Robotics and Computer-Integrated Manufacturing* 66, 101987. doi:10.1016/j.rcim.2020.101987

Min, S., Dornfeld, D., Inasaki, I., Ohmori, H., Lee, D., Deichmueller, M., et al. (2006). Variation in Machinability of Single Crystal Materials in Micromachining. *CIRP Ann.* 55 (1), 103–106. doi:10.1016/s0007-8506(07)60376-x

Molinari, A., Canova, G. R., and Ahzi, S. (1987). A Self Consistent Approach of the Large Deformation Polycrystal Viscoplasticity. *Acta Metallurgica* 35 (12), 2983–2994. doi:10.1016/0001-6160(87)90297-5

Parajuli, P., Mendoza-Cruz, R., Santiago, U., Ponce, A., and Yacamán, M. J. (2018). The Evolution of Growth, Crystal Orientation, and Grain Boundaries Disorientation Distribution in Gold Thin Films. *Cryst. Res. Tech.* 53 (8), 1800038. doi:10.1002/crat.201800038

Peng, L., Xu, Z., Gao, Z., and Fu, M. W. (2018). A Constitutive Model for Metal Plastic Deformation at Micro/meso Scale with Consideration of Grain Orientation and its Evolution. *Int. J. Mech. Sci.* 138-139, 74–85. doi:10.1016/j.ijmecsci.2017.11.046

Puchicabrera, E., Villalobosgutierrez, C., Irausquin, I., Labarberasosa, J., and Mesmacque, G. (2006). Fatigue Behavior of a 7075-T6 Aluminum alloy Coated with an Electroless Ni-P deposit. *Int. J. Fatigue* 28 (12), 1854–1866. doi:10.1016/j.ijfatigue.2005.12.005

Riyad, I. A., Feather, W. G., Vasilev, E., Lebensohn, R. A., McWilliams, B. A., Pilchak, A. L., et al. (2021). Modeling the Role of Local Crystallographic Correlations in Microstructures of Ti-6Al-4V Using a Correlated Structure Visco-Plastic Self-Consistent Polycrystal Plasticity Formulation. *Acta Materialia* 203, 116502. doi:10.1016/j.actamat.2020.116502

Roatta, A., Leonard, M., Nicoletti, E., and Signorelli, J. W. (2021). Modeling Texture Evolution during Monotonic Loading of Zn-Cu-Ti alloy Sheet Using the Viscoplastic Self-Consistent Polycrystal Model. *J. Alloys Comp.* 860, 158425. doi:10.1016/j.jallcom.2020.158425

Schmid, E., and Boas, W. (1950). *Plasticity of Crystals*. Cambridge, UK: University of cambridge.

Simoneau, A., Ng, E., and Elbestawi, M. A. (2007). Grain Size and Orientation Effects when Microcutting AISI 1045 Steel. *CIRP Ann.* 56 (1), 57–60. doi:10.1016/j.cirp.2007.05.016

Sun, L., Chen, M.-h., and Zhang, L. (2019). Microstructure Evolution and Grain Orientation of IMC in Cu-Sn TLP Bonding Solder Joints. *J. Alloys Comp.* 786, 677–687. doi:10.1016/j.jallcom.2019.01.384

Sun, Y., Su, Z., Gong, Y., Ba, D., Yin, G., Zhang, H., et al. (2021). Analytical and Experimental Study on Micro-grinding Surface-Generated Mechanism of DD5 Single-crystal Superalloy Using Micro-diamond Pencil Grinding Tool. *Archiv. Civ. Mech. Eng.* 21 (1). doi:10.1007/s43452-020-00163-6

Tabei, S. B. (2015). Modeling of Microstructural Evolutions in Machining of Dual Phase Alloys. Dissertation. Atlanta, GA: Georgia Institute of Technology.

Tang, T., Zhou, G., Li, Z., Li, D., Peng, L., Peng, Y., et al. (2019). A Polycrystal Plasticity Based Thermo-Mechanical-Dynamic Recrystallization Coupled Modeling Method and its Application to Light Weight Alloys. *Int. J. Plasticity* 116, 159–191. doi:10.1016/j.ijplas.2019.01.001

Wang, Q., Shankar, R. M., and Liu, Z. (2021). Visco-plastic Self-Consistent Modeling of Crystallographic Texture Evolution Related to Slip Systems Activated during Machining Ti-6AL-4V. *J. Alloys Comp.* 853, 157336. doi:10.1016/j.jallcom.2020.157336

Wu, C., Pang, J., Li, B., and Liang, S. Y. (2019). High-speed Grinding of HIP-SiC Ceramics on Transformation of Microscopic Features. *Int. J. Adv. Manuf Technol.* 102 (5-8), 1913–1921. doi:10.1007/s00170-018-03226-4

Wu, X., Li, L., He, N., Zhao, M., and Zhan, Z. (2015). Investigation on the Influence of Material Microstructure on Cutting Force and Bur Formation in the Micro Cutting of Copper. *Int. J. Adv. Manuf Technol.* 79 (1-4), 321–327. doi:10.1007/s00170-015-6828-5

Xiao, G., Song, K., He, Y., Wang, W., Zhang, Y., and Dai, W. (2021). Prediction and Experimental Research of Abrasive belt Grinding Residual Stress for Titanium alloy Based on Analytical Method. *Int. J. Adv. Manuf Technol.* 115 (4), 1111–1125. doi:10.1007/s00170-021-07272-3

Xie, H., Li, W.-l., Zhu, D.-H., Yin, Z.-p., and Ding, H. (2020). A Systematic Model of Machining Error Reduction in Robotic Grinding. *Ieee/asme Trans. Mechatron.* 25 (6), 2961–2972. doi:10.1109/tmech.2020.2999928

Yasakau, K. A., Tedim, J., Zheludkevich, M. L., and Ferreira, M. G. S. (2014). "Smart Self-Healing Coatings for Corrosion protection of Aluminium Alloys," in *Handbook of Smart Coatings for Materials Protection*. Editor A. S. H. Makhlouf (United Kingdom: Woodhead Publishing), 224–274. doi:10.1533/9780857096883.2.224

Zhang, M.-c., Zhang, Q., and Wei, K. (2018). The Correlation between Grain Orientation Evolution and Stress Rupture Properties of Waspaloy. *Metall. Mat Trans. A.* 49 (12), 6063–6074. doi:10.1007/s11661-018-4923-6

Zhang, N., Meng, L., Zhang, B., Han, Y., Yang, F., Ma, G., et al. (2021). Experimental Investigation and Simulation of Crystallographic Orientations Evolution in a Cold-Rolled Ultra-thin Grain-Oriented Silicon Steel. *J. Magnetism Magn. Mater.* 517, 167385. doi:10.1016/j.jmmm.2020.167385

Zhang, S. H., and Li, Z. G. (2008). Experimental Research on Grain Orientation Evolution of Extruded Mg Alloy AZ31B Sheet during Uniaxial Tensile Deformation. *Amr* 32, 87–92. doi:10.4028/www.scientific.net/amr.32.87

Zhao, M., Mao, J., Ji, X., Feng, Y., and Liang, S. Y. (2021). Effect of Crystallographic Orientation on Residual Stress Induced in Micro-grinding. *Int. J. Adv. Manuf Technol.* 112 (5-6), 1271–1284. doi:10.1007/s00170-020-06329-z

Zhu, D., Feng, X., Xu, X., Yang, Z., Li, W., Yan, S., et al. (2020). Robotic Grinding of Complex Components: A Step towards Efficient and Intelligent Machining - Challenges, Solutions, and Applications. *Robotics and Computer-Integrated Manufacturing* 65, 101908. doi:10.1016/j.rcim.2019.101908

Conflict of Interest: The authors declare that the research was conducted in the absence of any commercial or financial relationships that could be construed as a potential conflict of interest.

GLOSSARY

CO Crystallographic orientation

EBSD Electron back-scattered diffraction

FCC Face centered cubic

IPFs Inverse pole diagrams

ODF Orientation distribution function Notation

a_{ij} the constant and exponents

$\boldsymbol{A}$ the yield stress

$\boldsymbol{B}$ the coefficient of strain hardening

$\boldsymbol{C}$ the coefficient of strain rate hardening

$\boldsymbol{m}$ the thermal softening exponent

$\bar{M}^c$ the secant modulus

$\boldsymbol{n}$ the strain hardening exponent

$\boldsymbol{S}$ *the* fourth-order Eshelby tensor

T temperature

$\dot{T}$ temperature rate

T_0, T_m, T_w workpiece, melting and ambient temperature

$\boldsymbol{\delta}$ the randomly distributed error terms

ε Plastic strain

$\dot{\varepsilon}$ Plastic strain rate

$\dot{\varepsilon}_0$ Material constant

$\dot{\varepsilon}_{ij}^c$ the strain rate in the crystal

$\prod$ the skew-symmetric fourth-order Eshelby tensor

τ_{CRSS} critical resolved shear stress

$\boldsymbol{\Omega}_{ij}^c$ the rotation rate of the crystal